Band structures and alignment properties in ^{74}Se

J. Döring,[1,2] G. D. Johns,[1,*] M. A. Riley,[1] S. L. Tabor,[1] Y. Sun,[3,4]
and J. A. Sheikh[5]
[1]*Department of Physics, Florida State University, Tallahassee, Florida 32306*
[2]*Department of Physics, University of Notre Dame, Notre Dame, Indiana 46556*
[3]*Department of Physics and Astronomy, University of Tennessee, Knoxville, Tennessee 37996*
[4]*Department of Physics and Atmospheric Science, Drexel University, Philadelphia, Pennsylvania 19104*
[5]*Tata Institute of Fundamental Research, Colaba, Bombay, 400 005, India*
(Received 5 November 1997)

High-spin states in the even-even nucleus ^{74}Se were investigated via the ^{65}Cu(^{12}C, $p2n$)^{74}Se reaction at a beam energy of 50 MeV. On the basis of coincidence data three of the known bands were extended to higher spins and two new bands were found. Experimental crossing frequencies were deduced for various band structures and compared with cranked-shell-model results. Previous assignments of $g_{9/2}$ quasiproton and $g_{9/2}$ quasineutron alignments along the yrast line were confirmed when a near-prolate shape is assumed. Hartree-Fock-Bogoliubov calculations predict a deformed shape for excited states in ^{74}Se which shows, however, a considerable softness in triaxiality. For the first time in the mass 70 region, band structures and quasiparticle alignments in ^{74}Se were also investigated using the projected shell model. The calculations support the previous conclusions for the positive-parity states and predict that the lowest negative-parity bands are signature partners based on $g_{9/2}$ quasiproton excitations, with a $g_{9/2}$ quasineutron crossing at higher frequencies leading to a four-quasiparticle configuration at high spins. [S0556-2813(98)03906-5]

PACS number(s): 21.10.Re, 21.60.Cs, 23.20.Lv, 27.50.+e

I. INTRODUCTION

Properties of high-spin states in the neutron deficient even-even Se isotopes were studied extensively in the past and different explanations for the irregularities observed along the yrast positive-parity band were published [1–10]. The low-spin anomaly in the yrast bands of ^{70,72,74}Se is well known and has been interpreted in a shape coexistence picture of two bands with different deformations [2,4,7]. The effect observed in ^{72,74}Se has also been interpreted in the framework of an interacting boson approach [6,9] without any special assumption about the nuclear shape or shape coexistence.

More recently, the yrast bands of ^{70,72}Se were investigated [11] up to spins and parities of (16^+) and (28^+), respectively. In particular, the absence of any sharp backbending after the low-spin anomaly along the yrast band in ^{72}Se was interpreted as due to a strong yrast-yrare interaction at prolate deformation causing a gradual alignment of two-quasiprotons and two-quasineutrons in the unique-parity $g_{9/2}$ orbitals. In the same way, however with different interaction strength, the pronounced upbends observed in the yrast bands of the heavier isotopes ^{76,78}Se [12–14] were interpreted as due to the interaction of the ground-state band with two-quasiproton and two-quasineutron $g_{9/2}$ excitations.

The high-spin level scheme of ^{74}Se has been most recently studied [10] and the yrast band and three other bands have been extended to higher spin states. In particular, the yrast band has been tentatively observed up to a 24^+ level, where the two highest levels contribute to an unusually strong upbend in the kinematic moments of inertia (see Fig. 7 in Ref. [10]). Moreover, the band containing the levels at 1268.9 and 1884.0 keV has been reinterpreted [10] as a second $K^\pi=0^+$ band built on the second 0^+ level at 853.9 keV excitation energy. In this interpretation the larger moment of inertia would force this second 0^+ band to become yrast above spin 12 and would cause a band interaction or crossing which has not been found, so far. Therefore, we decided to reinvestigate ^{74}Se at high spins with a thin target coincidence experiment and a larger Ge detector array.

II. EXPERIMENTAL PROCEDURE AND RESULTS

The experiment was carried out using the ^{65}Cu(^{12}C, $p2n$)^{74}Se reaction at a beam energy of 50 MeV. The Cu target was a self-supporting foil of 0.6 mg/cm^2 enriched to 99% in ^{65}Cu. In this experiment the Pitt-FSU detector array [15], consisting of 9 Compton-suppressed high-purity Ge detectors with individual efficiencies of about 25%, was employed. Two detectors were placed at a forward angle of 35°, 3 detectors at 90°, and 4 detectors at a backward angle of 145°. The target to detector distance was chosen to be about 18 cm. About 5×10^7 prompt coincidence events were recorded on magnetic tape and sorted off-line into a total γ-γ matrix after gain correction for the Doppler shift of the γ rays. The dispersion used in this matrix was 0.8 keV/channel. Threefold events were decomposed into twofold events and subsequently stored in the matrix. The efficiency calibration of the Ge detectors was performed with a ^{152}Eu source placed at the target position. The γ-ray energies and intensities for transitions assigned to ^{74}Se are compiled in Table I.

Moreover, additional sorting of the ^{65}Cu+^{12}C data was carried out to determine directional correlations of oriented

*Present address: Los Alamos National Laboratory, Los Alamos, NM 87545.

TABLE I. Energies, relative intensities, and DCO ratios, as well as initial and final states of γ rays assigned to ^{74}Se.

E_γ [a] (keV)	I_γ [b]	R_{DCO} [c]	I_i^π [d]	I_f^π [e]	E^f (keV)	E_γ [a] (keV)	I_γ [b]	R_{DCO} [c]	I_i^π [d]	I_f^π [e]	E^f (keV)
219.3(1)	0.9(2)		0_2^+ [g]	2^+	853.9	1088.0(3)	16(1)	1.11(6)	11^-	9^-	5490.3
325.1(2)	2.3(2)	1.26(15)	7_2^-	7^-	3840.6	1135.2(6)	2(1)		(13_2^-)	(11_2^-)	7062.7
346.2(3)	1.2(2)			8^-	4543.9	1137.5(6)	2(1)		(12_2^+)	(10_2^+)	6014.3
368.5(2)	1.0(2)		(4_2^-)	4^-	3199.7	1151.0(2)	4.3(6)	0.75(10)	6^-	6^+	3382.1
399.2(3)	1.4(2)			6^-	3781.3	1157.8(5)	3.4(5)	0.96(11)	15^-	13^-	7843.8
445.5(3)	0.8(2)		(9_2^-)	9^-	4847.8	1186.9(3)	34(2)	1.03(6)	12^+	10^+	5442.6
481.5(3)	<1		4^-	3^-	2831.2	1192.9(6)	6(1)	1.10(11)	13^+	11^+	6685.5
492.8(1)	14(1)	0.98(4)	5^-	3^-	2842.3	1193.0(12)	3(1)		(14_2^+)	(12_2^+)	7205.9
511.0(3)	≈ 1		3^-	(2_3^+)	2349.4	1195.7(3)	10(2)	1.09(8)	13^-	11^-	6686.0
521.0(1)	1.7(3)		3^+	4^+	1884.0	1198.0(4)	4(1)	1.08(10)	14^-	12^-	7451.1
529.2(4)	<1		7^-	6_2^+	3515.4	1203.9(4)	<1		(2_3^+)	2^+	1838.4
539.8(2)	3.3(3)	0.29(8)	6^-	5^-	3382.1	1208.2(6)	2.3(5)	0.57(11)	15^+	14^+	7943.5
550.9(2)	4.8(4)	1.02(9)	6^-	4^-	3382.1	1236.7(5)	1.7(4)	0.34(9)	11^+	10^+	5492.5
571.7(3)	2.1(3)		(12_2^+)	12^+	6014.3	1243.1(6)	1.4(4)		13^+	12^+	6685.5
573.9(3)	2.2(4)			7^-	4089.3	1249.4(3)	4(1)	0.92(10)	3^+	2^+	1884.0
611.2(2)	7.2(7)	0.69(6)	5^-	6^+	2842.3	1251.2(4)	1.6(5)	0.66(14)	9^+	8^+	4449.3
615.1(1)	6.5(7)	0.68(6)	3^+	2_2^+	1884.0	1258.2(5)	4.9(4)	1.20(18)	15^+	13^+	7943.5
621.2(2)	3.2(4)	1.14(13)	(10_2^+)	10^+	4876.9	1268.9(2)	7.1(6)		2_2^+	0^+	1268.9
634.3(3)	≈ 12		2_2^+	2^+	1268.9	1284.4(3)	1.8(3)		7^-	6^+	3515.4
634.6(2)	≈ 120	0.99(3)	2^+	0^+	634.6	1291.8(4)	3(1)	0.90(10)	15_2^-	13^-	7977.8
657.0(3)	2.1(3)			9^-	5059.3	1292.4(4)	19(2)	1.05(8)	14^+	12^+	6735.0
673.1(1)	24(2)	0.99(3)	7^-	5^-	3515.4	1293.7(5)	3(1)		7^+	6^+	3525.0
682.1(3)	1.7(4)	$\leqslant 0.5$	8^-	7^-	4197.7	1298.6(3)	4.0(4)		5^+	4^+	2661.4
720.6(3)	2.3(5)	0.71(13)	6^-	5^+	3382.1	1321.6(4)	1.9(3)		(17^-)	15_2^-	9299.3
723(1)	<1		(4_2^-)	(2^-)	3199.7	1330.5(6)	4.2(8)		(16_2^+)	(14_2^+)	8536.5
728.3(2)	100(2) [h]	1.02(3)	4^+	2^+	1362.9	1350.4(6)	3.1(5)		(17^+)	15^+	9293.9
730.5(8)	3(2)		(8_2^+)	8^+	3928.6	1364.0(5)	2.1(3)	0.91(12)	16^-	14^-	8815.1
734.4(2)	15(1)	0.57(5)	5^-	4_2^+	2842.3	1381.1(4)	8.8(9)	1.10(9)	16^+	14^+	8116.1
744.7(3)	6.0(5)	0.70(10)	4_2^+	4^+	2107.8	1455.4(4)	1.9(3)	0.99(16)	17^-	15^-	9299.3
762.9(4)	1.0(3)				4543.9	1468.3(3)	6.8(9)	1.10(13)	4^-	4^+	2831.2
777.4(3)	6.1(5)	0.80(12)	5^+	3^+	2661.4	1473.3(3)	3.5(5)		4_2^+	2^+	2107.8
815.6(2)	12(1)	1.12(7)	8^-	6^-	4197.7	1479.5(3)	4.4(5)	0.64(11)	5^-	4^+	2842.3
838.9(2)	16(2)		4_2^+	2_2^+	2107.8	1532(1)	1.0(5)		(19^+)	(17^+)	10826
850.1(3)	2(1)		(4_2^-)	3^-	3199.7	1554.8(7)	1.5(5)		(18^-)	16^-	10369.9
863.6(3)	7.4(9)	0.97(14)	7^+	5^+	3525.0	1563.8(6)	4.9(4)	0.97(10)	18^+	16^+	9679.9
868.2(2)	81(3)	1.02(4)	6^+	4^+	2231.1	1591.5(7)	2.9(6)	1.21(18)	(18_2^+)	(16_2^+)	10128.1
878.4(3)	3.8(5)		6_2^+	4_2^+	2986.2	1609.6(4)	3.2(6)	0.59(11)	7_2^-	6^+	3840.6
886.9(2)	21(2)	1.04(5)	9^-	7^-	4402.3	1623.5(7)	3.6(7)	1.12(18)	6_2^+	4^+	2986.2
924.5(3)	10(1)	0.98(8)	9^+	7^+	4449.3	1626(1)	1.4(9)		(19^-)	17^-	10925
942.7(5)	1.1(3)		(8_2^+)	6_2^+	3928.6	1679(1)	≈ 1		(10_2^+)	8^+	4876.9
948.4(5)	2.4(3)		(10_2^+)	(8_2^+)	4876.9	1679.7(7)	2.5(8)	1.18(18)	20^+	18^+	11359.6
966.8(2)	56(2)	1.04(5)	8^+	6^+	3197.9	1698.4(12)	≈ 1		(8_2^+)	6^+	3928.6
984.5(2)	2.5(8)		(2_3^+)	0_2^+	1838.4	1714.9(4)	6.4(6)	0.50(4)	3^-	2^+	2349.4
986.3(2)	4.0(8)	0.58(8)	3^-	4^+	2349.4	1734(1)	1.4(5)		(20^-)	(18^-)	12104
1007.1(3)	4.7(7)		(9_2^-)	7_2^-	4847.8	1759(2)	≈ 1		(12_2^+)	10^+	6014.3
1011.0(3)	13(1)	0.87(10)	10^-	8^-	5208.7	1763.3(10)	1.6(4)	0.99(21)	(14_2^+)	12^+	7205.9
1043.2(3)	7(1)	0.92(9)	11^+	9^+	5492.5	1801.6(8)	0.8(3)	0.94(30)	(16_2^+)	14^+	8536.5
1044.4(3)	7(1)	1.11(8)	12^-	10^-	6253.1	1836.9(5) [i]	1.0(3)	0.80(23)	(4_2^-)	4^+	3199.7
1057.8(3)	46(2)	1.09(6)	10^+	8^+	4255.7	1842(1)	0.6(3)	0.81(23)	22^+	20^+	13202
1079.7(3)	4(1)		(11_2^-)	(9_2^-)	5927.5	1843.1(6) [i]	1.4(3)	0.99(19)	(2^-)	2^+	2477.7
1080.5(2)	7(1)	0.52(5)	3^-	2_2^+	2349.4						

[a] Errors in the last digit are shown in parentheses.
[b] Intensities deduced from the total matrix of the ^{65}Cu(^{12}C, $p2n$)^{74}Se measurement.
[c] DCO ratio; $R = I_\gamma(35°,145°)/I_\gamma(90°)$.
[d] Spin and parity of the initial state.
[e] Spin and parity of the final state.
[f] Initial state energy.
[g] Assignment taken from Ref. [7].
[h] Normalization.
[i] Deduced from thick target experiment, Ref. [10].

nuclei (DCO) ratios [16,17]. For this purpose a matrix was established where the events from the two forward and the four backward detectors were sorted against the 90° events (3 Ge detectors). The DCO ratio is determined from the experimental intensity ratio of a given transition according to $R_{\mathrm{DCO}}=I_\gamma(35°,145°)/I_\gamma(90°)$. In general, the DCO ratio depends on the initial and final spins and on the mixing ratio of different multipoles in the gating and in the transition of interest, as well as on the degree of nuclear alignment. When a gate is set on a stretched $\Delta I=2$ transition, then the interpretation of the experimental ratios is most straightforward. In this case the DCO ratio is expected to be about 1.0 and 0.5 for stretched $E2$ and pure $\Delta I=1$ transitions, respectively. If dipole-quadrupole mixing is included, then the DCO ratio for a $\Delta I=1$ transition may vary between 0.2 and 1.8 (depending also on the nuclear alignment), with the mixing ratio $\delta>0$ for $R_{\mathrm{DCO}}<0.5$ and $\delta<0$ for $R_{\mathrm{DCO}}>0.5$, respectively. Furthermore, for a pure dipole $\Delta I=0$ transition a DCO ratio of 1.10 is expected. This value is reduced smoothly (down to about 0.6) with increasing dipole-quadrupole mixing ($\delta\rightarrow\pm\infty$).

In the DCO matrix gates were set exclusively on transitions known to have $E2$ multipolarity from previous studies of ^{74}Se. In some cases several background-corrected gates set on stretched $E2$ transitions within a certain band were added together to improve the statistics. For most low-lying transitions, gates were set from above to avoid any, even the smallest, influence of the radioactive decay of ^{74m}Br $\rightarrow$ ^{74}Se. (In general, for a very thin target all recoils fly away.) Wherever possible, different gates or combinations were used to extract the DCO ratios. Therefore, the results given in Table I represent average values. In general, most of the DCO ratios are in fair agreement with those of Ref. [10] although the errors quoted here are somewhat smaller due to better statistics. The most significant difference is for the 615.1 keV line where gating from above yields a DCO value of 0.68(6) supporting a $\Delta I=1$ nature for this transition.

It should be mentioned that the DCO ratios for the $\Delta I=1$ $E1$ transitions at 611.2 and 720.6 keV are somewhat larger than expected ($\approx$0.5) from theory. Similarly, the DCO ratio for the 1151.0 keV $E1$ transition is somewhat too small for a pure $\Delta I=0$ character. However, the assumption of small $M2$ components in these three transitions seems to be very unlikely.

III. LEVEL SCHEME OF ^{74}Se

The level scheme deduced from our coincidence measurement is shown in Fig. 1. It contains several newly introduced levels and changes compared to the predecessors. Therefore, some details will be discussed next.

A. Positive-parity states

The present coincidence results have confirmed the states up to spin 20^+ reported [10] for the yrast band, band 2 in Fig. 1, and a new 22^+ state at 13202 keV has been added. The tentatively proposed transitions at 1761.7 and 1800.6 keV introduced in Ref. [10] to feed into the (20^+) state have been found to depopulate a weakly excited sideband, band 3, and to feed into the 12^+ and 14^+ states of the yrast band rather than to be the high-spin extension. Neither transition is in coincidence with the 1381.1 keV (see Fig. 2) or higher-lying transitions in the yrast sequence. From our data an 1842 keV transition is proposed as the decay from the new 22^+ state, as can be seen in the coincidence gate at 1381.1 keV γ-ray energy.

The upper part of the weakly populated sideband 3, likely of positive parity, has been observed for the first time. The lowest state of this structure is very probably the (8^+) level at 3928.6 keV. This state decays by three low-intensity transitions. One of them is a 942.7 keV transition feeding into the 6_2^+ state at 2986.2 keV of the γ-vibrational band [7,10,18]. The even-spin members of the γ-vibrational band are built on the second 2^+ state at 1268.9 keV and are shown as the lower part of band 3 in Fig. 1. The (10^+) and (12^+) states of band 3 decay, in addition to the intraband transitions, via $\Delta I=0$ γ rays at 621.2 and 571.7 keV, respectively, to the nearest states of the yrast band. Both interband transitions can be seen clearly in the coincidence spectra shown in Fig. 3. The higher-lying (14^+), (16^+), and (18^+) levels of band 3 depopulate by $\Delta I=2$ transitions only. Here the $\Delta I=0$ transitions have not been observed. DCO ratios could be determined for only a few of the transitions in this weak band, precluding firm spin assignments. The DCO ratios for the 621.2, 1591.5, 1763.3, and 1801.6 keV lines (see Table I) are consistent with $\Delta I=0$ or $\Delta I=2$ decay and with the suggested spins.

The 4_2^+ level at 2107.8 keV and the 6_2^+ level at 2986.2 keV are known from previous work as members of the γ-vibrational band. Their spin assignments could be confirmed, and an additional decay path via the 1623.5 keV γ ray to the yrast 4^+ state has been observed. It seems that this even-spin sequence is only weakly populated in our experiment compared to the odd-spin signature partner, band 1 in Fig. 1. The odd-spin sequence is built on top of the 3^+ level at 1884.0 keV and has been observed up to a 10826 keV state with a tentative spin 19. Here we have been able to add three new transitions.

In the past different spin assignments were given for the 1884.0 keV level and the sequence built on it. Based on angular distribution and DCO measurements [7,18] spin and parity of 3^+ were assigned to this state. However, the possibility of a spin 4 was not completely ruled out. The assignment was later changed [10] to 4^+ due to the measured DCO ratios of the 615.1 and 1249.4 keV transitions. However, since the 1884.0 keV level is strongly populated in the radioactive decay of the ^{74}Br high-spin isomer, these DCO results should be treated with caution especially when gated from below in a thick target experiment. Recently, a spin of 3 was firmly assigned based on the anisotropy coefficients deduced from a low-temperature nuclear orientation measurement [19] following the decay of ^{74m}Br. The spin 3 assignment is confirmed in the present work by the DCO ratio of 0.68(6) for the 615.1 keV γ ray. This value has been obtained by gating from above, i.e., from the analysis of a spectrum gated by the 777.4 and 924.5 keV transitions. Moreover, the DCO ratios for the 1208.2, 1236.7, and 1251.2 keV higher-lying transitions linking this sequence to the yrast band indicate a $\Delta I=1$ multipolarity for each transition. The measured DCO ratio of 0.92(10) for the 3^+

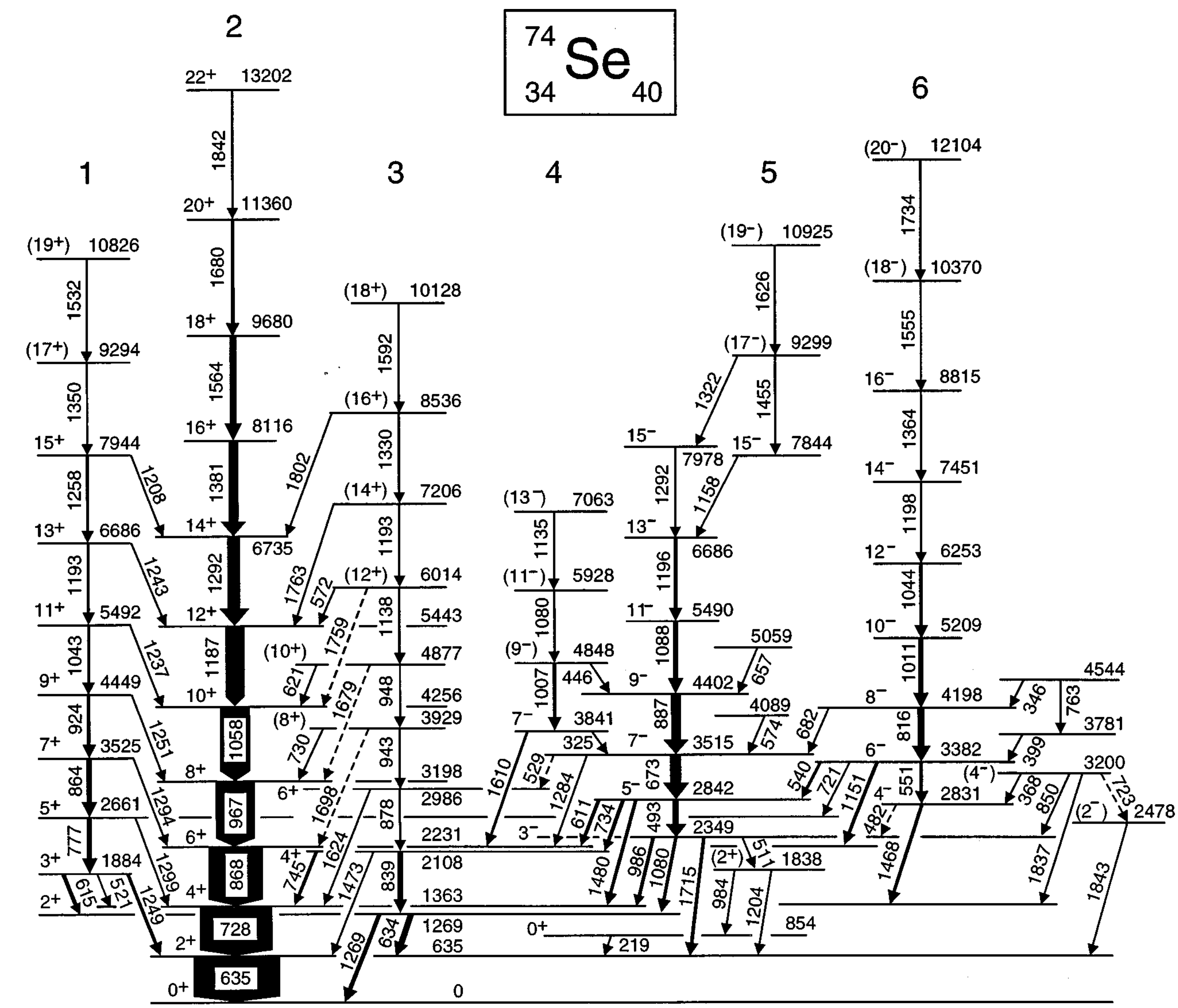

FIG. 1. Level scheme of ^{74}Se as obtained in the present study. The thickness of the arrow indicates the transition intensity.

$\rightarrow$ 2^+ 1249.4 keV transition can be explained with a mixed dipole-quadrupole nature of the transition.

The previous 4^+ assignment to the 1884.0 keV level would also lead to an intensity problem for the higher-lying states. Based on our DCO ratios, the transitions involved in band 1 carry $E2$ multipolarity and, thus, the state at 6685.5 keV would have a 14^+ assignment. This state would then be yrast, as well as the higher-lying states of this sequence. However, the population of these states is much less intense than that of the 14^+, 16^+, and 18^+ states at 6735.0, 8116.1, and 9679.9 keV in band 2, respectively. All together, the observations fit if we return to the former suggestion of 3^+ for the level at 1884.0 keV.

B. Negative-parity states

The negative-parity sequence, band 5, built on the 3^- state at 2349.4 keV was extended by several transitions up to a 10925 keV state with a tentative spin of 19. The previously suggested 15^- state at 7977.8 keV could be confirmed. Moreover, an additional lower-lying 15^- state at 7843.8 keV has been found, pointing to a band crossing in this sequence.

A new negative-parity sequence, band 4, was identified on top of the 3840.6 keV 7^- level. This level was already known from the observation of a 325.8 keV transition [7] in coincidence with the lower-lying members of the 3^- band. We found in addition a 1609.6 keV γ ray decaying from this state to the 6^+ member of the yrast band. The 9^- member of this new band decays, in addition to the 1007.1 keV intraband transition, via a weak 445.5 keV γ ray to the 9^- member of the 3^- band. The occurrence of this new band 4 in ^{74}Se is very similar to that of a recently found band in the isotone ^{76}Kr, labeled as band 4 in Ref. [20]. However, in ^{76}Kr the band starts at a 5^- state not seen in ^{74}Se.

The even-spin negative-parity sequence, band 6, built on the 4^- level at 2831.2 keV was extended by three new transitions at energies of 1364.0, 1554.8, and 1734 keV. The highest spin observed in this band is now tentatively 20. Based on the measured DCO ratios the spins assigned previously could be confirmed, and in conjunction with the $E1$ multipolarity for the 1468.3 keV γ ray given in Ref. [9] negative parity has been well established. A few additional sidefeeding transitions of 368.5, 399.2, and 346.2 keV have

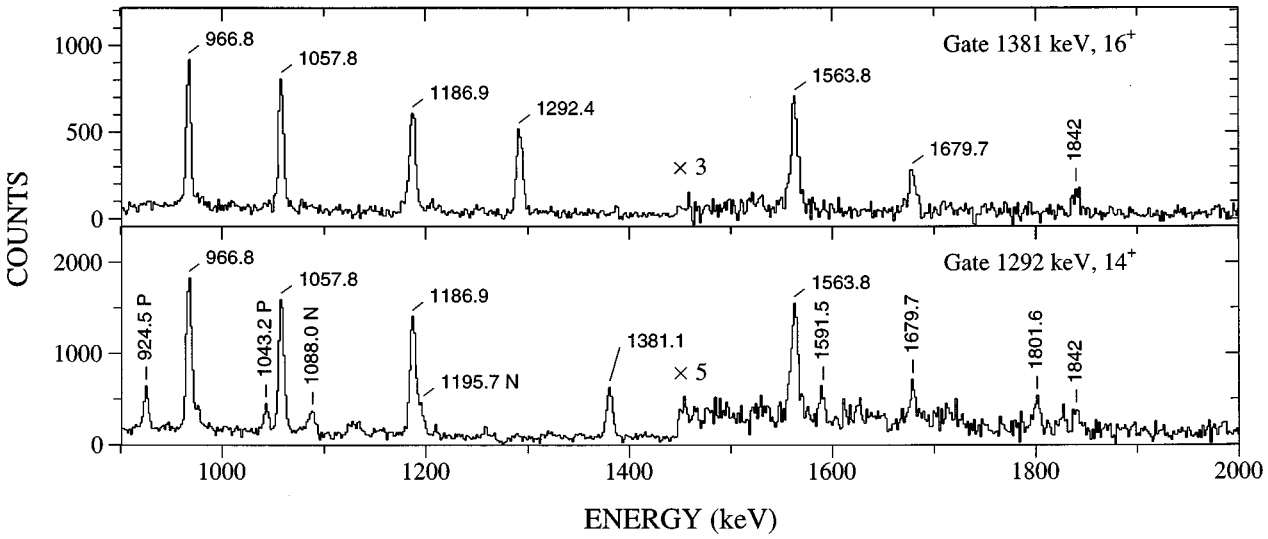

FIG. 2. Portions of background-corrected coincidence spectra obtained by gating in the total coincidence matrix on the γ rays at 1292 and 1381 keV of the yrast sequence, band 2. Since the 1292 keV peak is a triplet coincidences arising from the other γ rays belonging to the odd-spin positive-parity band 1 and the negative-parity band 5 are marked with the symbols P and N, respectively. Note the changes in scale at a γ-ray energy of about 1450 keV.

been identified. The level at 3199.7 keV (in decay work at 3200.8 keV) was already known from the ^{74m}Br decay by the observation of a 1837.6 keV transition feeding the 4^+ state [21]. The existence of this transition and of the 850.1 keV γ ray is confirmed in the present work, and also from the original coincidence matrices of the ^{58}Ni + ^{19}F thick target experiment of Ref. [10]. In the isotone ^{76}Kr the second 4^- state appears to be a bandhead for another high-spin sequence, band 5 in Ref. [20]. However, a similar band in ^{74}Se could not be found.

There is experimental evidence for a low-lying state at 2477.7 keV not seen in the β-decay studies [21]. This level decays via an 1843.1 keV transition to the 2^+ state, clearly seen in the 635 keV gate of the thick ^{58}Ni + ^{19}F experiment [10] where the top 1842 keV transition from the yrast sequence is completely Doppler shifted. Furthermore, the line is not seen in the 728 keV gate of that experiment. The measured DCO ratio points to a $\Delta I=0$ or 2 transition. A level closest to this energy, at 2482 keV, was reported previously from a (p,t) reaction study [22] with a spin and parity assignment of (2^+). The new level lies about 353 keV below the 4^- state but no connecting transition has been seen. However, there might be a population by a weak 723 keV transition from the second (4^-) state pointing to negative parity for the 2477.7 keV level.

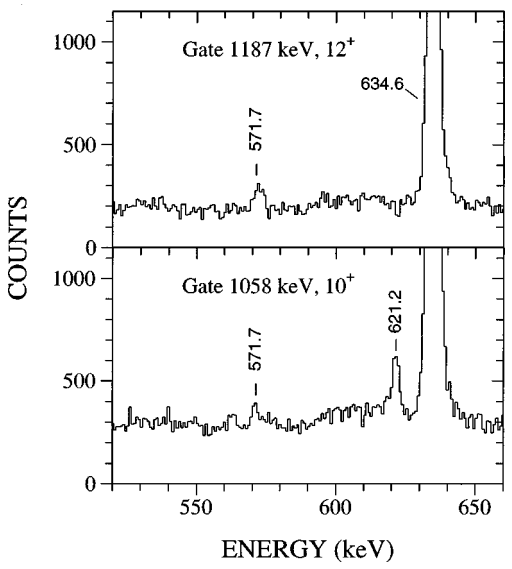

FIG. 3. Portions of background-corrected coincidence spectra obtained by gating on the 1058 and 1187 keV yrast-band transitions. The $\Delta I=0$ transitions are indicated by their energies. The peak at 634.6 keV is partly off the scale.

IV. DISCUSSION

A. Alignments in the yrast band and positive-parity sidebands

The yrast band of positive parity was identified up to a 22^+ state at 13202 keV. For most of the $E2$ transitions a high collectivity of about $B(E2)=38$ to 118 Weisskopf units (W.u.) was found [7,9,10] resulting in an average quadrupole deformation of about $\beta_2=0.30$ if axial symmetry is assumed.

The occurrence of a low-lying second 0^+ state at 853.9 keV and its decay to the yrast 2^+ state via a 219.3 keV transition with $B(E2)=82(6)$ W.u. [23] were interpreted in a shape coexistence picture [4,7] in which the ground state is weakly deformed, while the rotational band connected with the second 0^+ state contains the yrast 6^+, 8^+, and 10^+ states and is considered to be strongly (prolate) deformed. The 2^+ and 4^+ states of this strongly deformed 0_2^+ band are heavily disturbed by their interaction with the low-spin members of the less deformed ground-state band which is thought to be built on vibrational excitations [2,7]. This shape coexistence picture was developed due to the large similarities at low-spins between ^{74}Se and ^{72}Se. However, it seems that the structure of the positive-parity yrast band above the 8^+ state in ^{74}Se is more complicated, as already

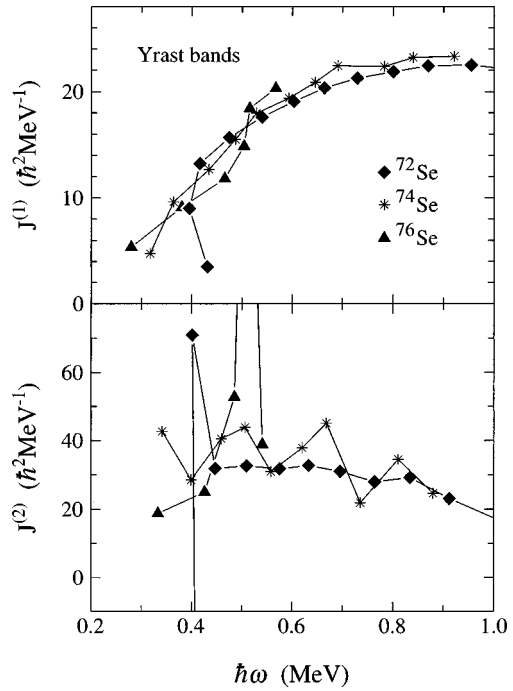

FIG. 4. Kinematic moments of inertia, $J^{(1)}$ (top), and dynamic moments of inertia, $J^{(2)}$ (bottom), for the positive-parity yrast bands in ^{72,74,76}Se as a function of the rotational frequency. The data were taken from ^{72}Se, Ref. [11] and ^{76}Se, Refs. [12,13]. A value of $K=0$ was used for all bands.

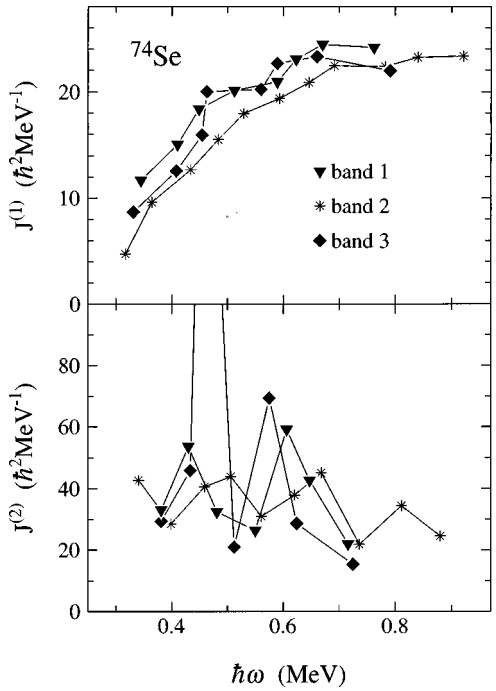

FIG. 5. Kinematic moments of inertia, $J^{(1)}$ (top), and dynamic moments of inertia, $J^{(2)}$ (bottom), for the positive-parity bands built on the ground state (band 2), on the second 2^+ state at 1268.9 keV (band 3), and on the 3^+ state at 1884.0 keV (band 1), as a function of the rotational frequency. In the analysis a value of $K=0$ was used for band 2 and $K=2$ for bands 1 and 3.

pointed out [3,7,8] in conjunction with the observed irregularity in the moments of inertia at spin 10. This irregularity corresponds to the first (weak) peak in the dynamic moment of inertia, $J^{(2)}$, at a rotational frequency of about 0.5 MeV as shown in Fig. 4. This peak is even more pronounced in the yrast bands of the heavier neighbors ^{76,78}Se whereas in the isotope ^{72}Se a smooth behavior occurs after the low-spin anomaly. It was suggested earlier [3] that this irregularity at 0.5 MeV in ^{74}Se is due to an unobserved band crossing with a band having a larger moment of inertia, i.e., after $g_{9/2}$ quasiparticle (qp) alignment has occurred, later identified as a $g_{9/2}$ quasiproton alignment [8]. However, there was at that time no additional experimental evidence for another high-spin band. In the present study it is shown that the irregularity in the yrast band is caused by its interaction with the new band 3. Analysis of the crossing frequencies supports the conclusion that the peak in the dynamic moment of inertia at 0.5 MeV is caused by an alignment of $g_{9/2}$ quasiprotons [8] if a near-prolate shape is assumed. Hence, the nonyrast band 3 which is thought to have a 2qp structure too is, therefore, predominantly based on $g_{9/2}$ quasineutron excitations.

The new band 3 built on top of the (8_2^+) level at 3928.6 keV is connected through a 942.7 keV transition to the even-spin members of the known γ-vibrational band which is shown as the low-spin extension of band 3 in the level scheme of Fig. 1, similar to the observation in band 1 where the odd-spins states are connected through a 924.5 keV transition. The kinematic and dynamic moments of inertia of the yrast band 2 and bands 1 and 3 are shown in Fig. 5 as a function of the rotational frequency. Both bands, 1 and 3, start off with a larger kinematic moment of inertia compared to the yrast band 2. The peaks in the dynamic moments of inertia at about 0.45 MeV for bands 1 and 3 (at the 924.5 and 942.7 keV transitions) are considered to be due to the change in structure, from vibrational to qp excitations. The next peak in the dynamic moments of inertia for bands 1 and 3 at about 0.6 MeV rotational frequency (see Fig. 5 bottom) indicates that the bands undergo qp alignment. Thus, a $g_{9/2}$ quasiproton crossing seems to be likely for band 3 at around spin 14 leading to a 4qp structure.

As can be seen in Fig. 5, there are two more (weak) peaks in the dynamic moment of inertia of the yrast band in ^{74}Se, at frequencies of 0.65 and 0.8 MeV, which can be related to additional qp alignments along the yrast line. The second crossing at 0.65 MeV is very likely due to a $g_{9/2}$ quasineutron crossing [8] if a near-prolate shape is still present. Thus, the yrast states above the 16^+ level are 4qp excitations. It should be noted that the strong upbend in the kinematic moments of inertia for the yrast band in ^{74}Se as shown in Fig. 7 of Ref. [10] has disappeared due to the new transition energies found in our study.

To investigate the dependence of the crossing frequencies on the nuclear shape, cranked-shell-model calculations [24] have been performed for different shape parameters. In this way, theoretical $g_{9/2}$ quasiproton and $g_{9/2}$ quasineutron crossing frequencies have been deduced. The results are shown in Fig. 6 where those frequencies are displayed as a function of the quadrupole deformation (left-hand side) and as a function of the triaxiality (right-hand side) for protons ($Z=34$) and neutrons ($N=40$). At a prolate deformation of 0.30, the $g_{9/2}$ quasiproton and quasineutron crossing frequencies are predicted to be 0.53 and 0.63 MeV, respectively. The calculated quasiproton-quasineutron frequency separation is about 0.1

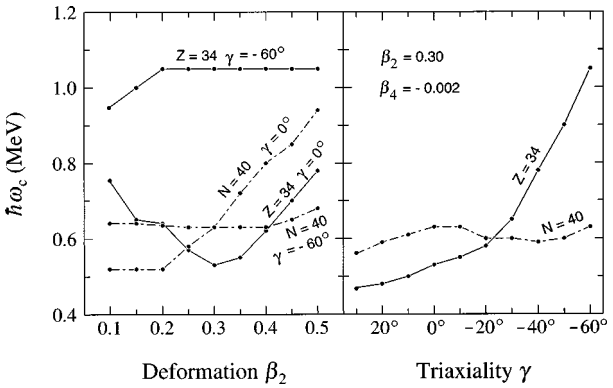

FIG. 6. Calculated crossing frequency, $\hbar\omega_c$, for the positive-parity yrast band as a function of the quadrupole deformation for collective prolate ($\gamma=0°$) and collective oblate ($\gamma=-60°$) shapes (left-hand side), and as a function of the triaxiality parameter γ for a fixed quadrupole deformation (right-hand side).

MeV at prolate deformation. It becomes smaller as the triaxiality moves towards negative γ values, reaching an equal frequency of 0.60 MeV at $\gamma=-22°$. At an oblate shape with $|\beta_2|=0.30$ the quasiproton crossing frequency is far above the quasineutron one. These calculations support the interpretation that the first and second crossings observed along the yrast line in ^{74}Se at 0.5 and 0.65 MeV can be ascribed to $g_{9/2}$ quasiproton and $g_{9/2}$ quasineutron alignments as long as the shape is considered to be near prolate.

This interpretation is supported by the systematics of crossing frequencies derived from the positive-parity bands observed in the odd-mass neighbors and blocking arguments. In the case of the odd-proton nuclei ^{73,75}Br [25] a $g_{9/2}$ quasineutron crossing frequency of $\hbar\omega_c^n=0.65$ MeV has been deduced from the favored positive-parity sequence. Likewise, the odd-neutron ^{75}Se isotope [26] exhibits $g_{9/2}$ quasiproton frequencies of $\hbar\omega_c^p=0.56$ and 0.48 MeV for the favored and unfavored positive-parity sequences, respectively.

B. Alignments in the negative-parity bands

Prior to this study the 3^- level at 2349.4 keV was discussed [23] as a collective octupole state due to its large $B(E3)$ decay strength of 9.2 W.u. to the ground state. For the $\Delta I=2$ γ-ray sequence built on top of this state, band 5 in Fig. 1, and observed up to (11^-) in Ref. [5] and up to (15^-) in Ref. [10], $E2$ transition probabilities between 51 and 78 W.u. were inferred from lifetimes measurements (see compilation in Ref. [9]). Even larger transition strengths (up to 104 W.u.) were deduced in Ref. [10]. The high collectivity was taken as evidence for an octupole rotational band of negative parity in ^{74}Se [5].

The even-spin sequence of negative parity, band 6, starts off with the 4^- state at 2831.2 keV and has been observed up to a (20^-) level at 12104 keV. For the negative-parity states up to spin 10 the measured lifetimes revealed collective $E2$ intraband transitions with $B(E2)$ values between 30 and 70 W.u. [9]. This high collectivity may be understood in terms of a rotation-aligned band built on the 4^- state which has a predominantly 2qp structure.

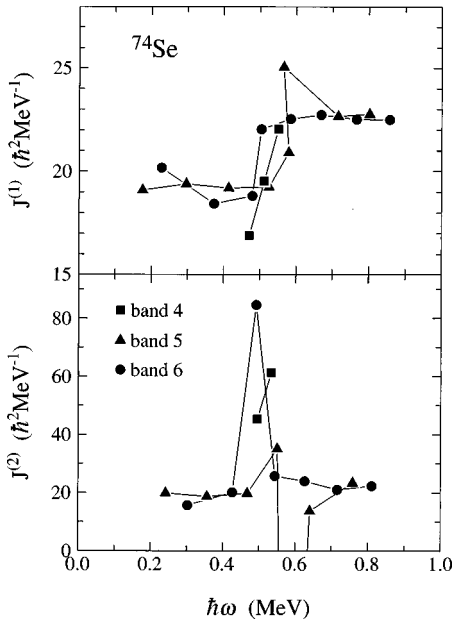

FIG. 7. Kinematic moments of inertia, $J^{(1)}$ (top), and dynamic moments of inertia, $J^{(2)}$ (bottom), for the three negative-parity bands 4, 5, and 6 as a function of the rotational frequency. For all three bands a value of $K=3$ was used. In the odd-spin band 5, the lowest 15^- state was taken which causes a large negative dynamic moment of inertia off the range displayed.

The kinematic and dynamic moments of inertia deduced from the experimental level energies for the negative-parity bands are shown in Fig. 7. Sharp upbends or downbends occur at rotational frequencies of about 0.55, 0.6, and 0.5 MeV in bands 4, 5, and 6, respectively.

In general, the negative-parity bands are based on octupole and 2qp excitations. The drastic changes in the moments of inertia along the bands can be related to additional $g_{9/2}$ qp alignments which lead to a 4qp structure in each band for states above the 10^- or 11^- states. However, the clear distinction between $g_{9/2}$ quasiproton and $g_{9/2}$ quasineutron excitations as outlined before for the yrast sequence in ^{74}Se as well as seen in ^{76}Kr [20] seems to have disappeared in ^{74}Se. It is very likely that bands 5 and 6 are signature partners, even though they have slightly different crossing frequencies. The difference between bands 5 and 6 is about the same as the quasineutron-quasiproton frequency difference at near-prolate shape prohibiting any structural conclusion on this basis. The problem might be related to the considerable γ-softness of the nucleus.

C. Shape calculations

To investigate the predicted nuclear shape of ^{74}Se at high spins, Hartree-Fock-Bogoliubov calculations were performed using the method outlined in Refs. [10,27]. The calculations were carried out with a Woods-Saxon potential for the single-particle energies and a monopole type pairing force. Total Routhian surfaces (TRS) calculated for the positive-parity yrast sequence at two different rotational frequencies are displayed in Figs. 8(a) and 8(b). The plot at 0.404 MeV rotational frequency which corresponds to a spin of about 6, depicts a situation just after the low-spin anomaly and before the anticipated band crossing. At this point, the available

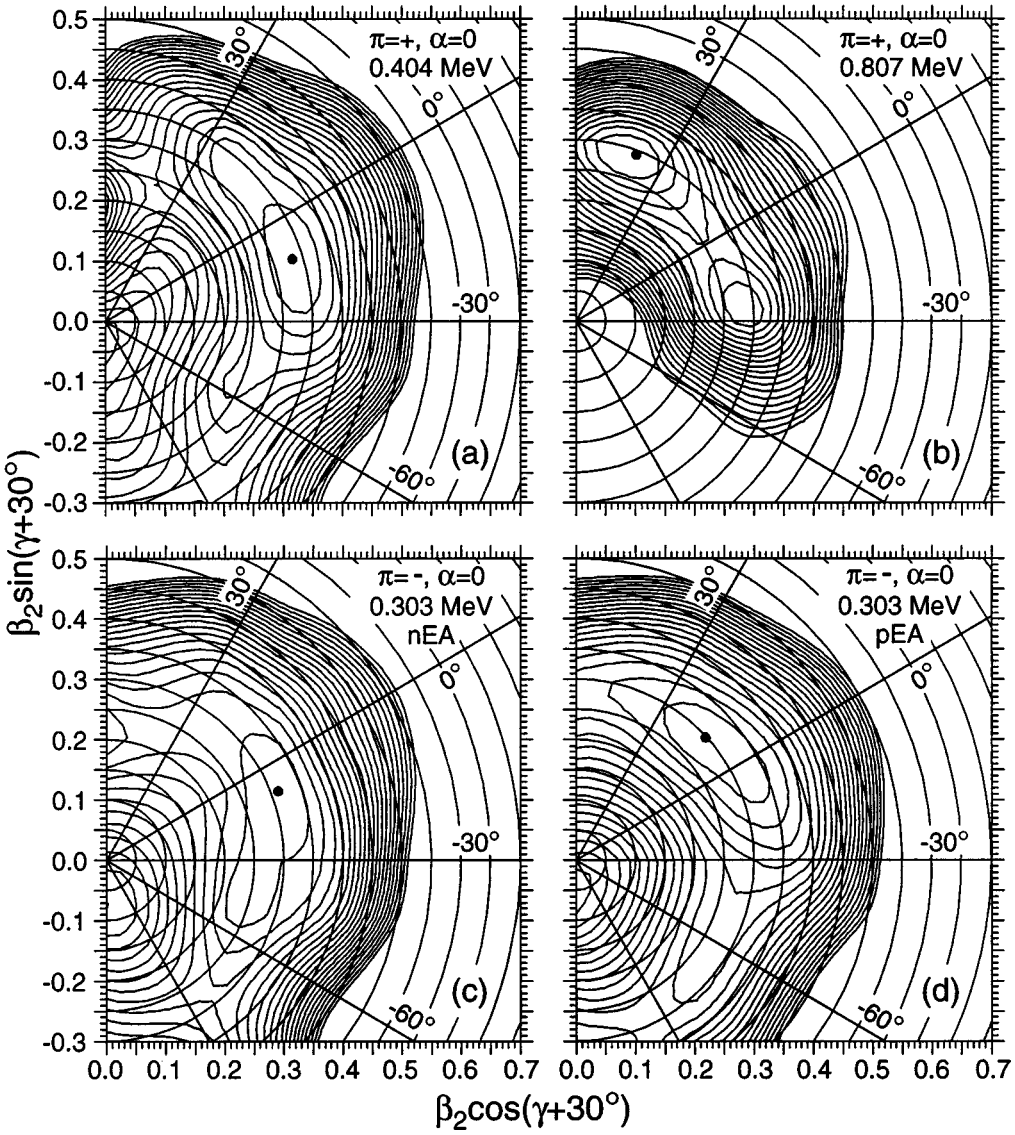

FIG. 8. Total Routhian surfaces for ^{74}Se in the (β_2,γ) plane for positive-parity states, (a) and (b). Negative-parity two-quasineutron and two-quasiproton surfaces are displayed in (c) and (d), respectively, for configurations with signature $\alpha=0$ at different rotational frequencies. The energy separation between contour lines is 200 keV.

amount of rotational energy has driven the nucleus to a near-prolate shape with $\beta_2=0.33$ and $\gamma=-12°$, away from the low-spin shape coexistence. At higher rotational frequency (at about a spin of 12), i.e., after the first qp alignment has occurred, the near-prolate minimum has evolved towards a triaxial shape which was illustrated already in Fig. 8 of Ref. [10]. The alignment of $g_{9/2}$ quasiprotons obviously drives the system towards positive γ values in agreement with earlier findings [27] for Kr isotopes, and another triaxial minimum appears. Even after the second alignment the system remains at a triaxial shape as can be seen for a rotational frequency of 0.807 MeV in Fig. 8(b). There are now two minima in the energy surface, one with $\beta_2=0.29$, $\gamma=40°$ and another one with $\beta_2=0.29$, $\gamma=-26°$. Both minima are very close in energy. However, it is very likely that the shape at the high-spin yrast states is represented by the collective triaxial minimum at $\gamma=-26°$.

Shape calculations were also performed for negative-parity configurations. Two sample TRS plots are shown in Figs. 8(c) and 8(d) for the two-quasineutron configuration EA with signature $\alpha=0$ and the two-quasiproton configuration EA with $\alpha=0$ at a rotational frequency of 0.303 MeV. The quasineutron and quasiproton TRS plots look rather similar with regard to the predicted shape, i.e., they show a considerable softness of the nuclear shape with regard to the triaxiality parameter γ. This might be the reason that no clear configuration assignment could be made on the basis of crossing frequencies.

D. Calculations by the projected shell model

1. Theory

In this section the projected-shell-model theory is briefly introduced as used for the interpretation of high-spin states in ^{74}Se. A more detailed description of the model can be found in a recent review article [28]. The projected shell model is a spherical shell model truncated in a deformed (Nilsson-type) BCS single-particle basis. More precisely, the truncation is

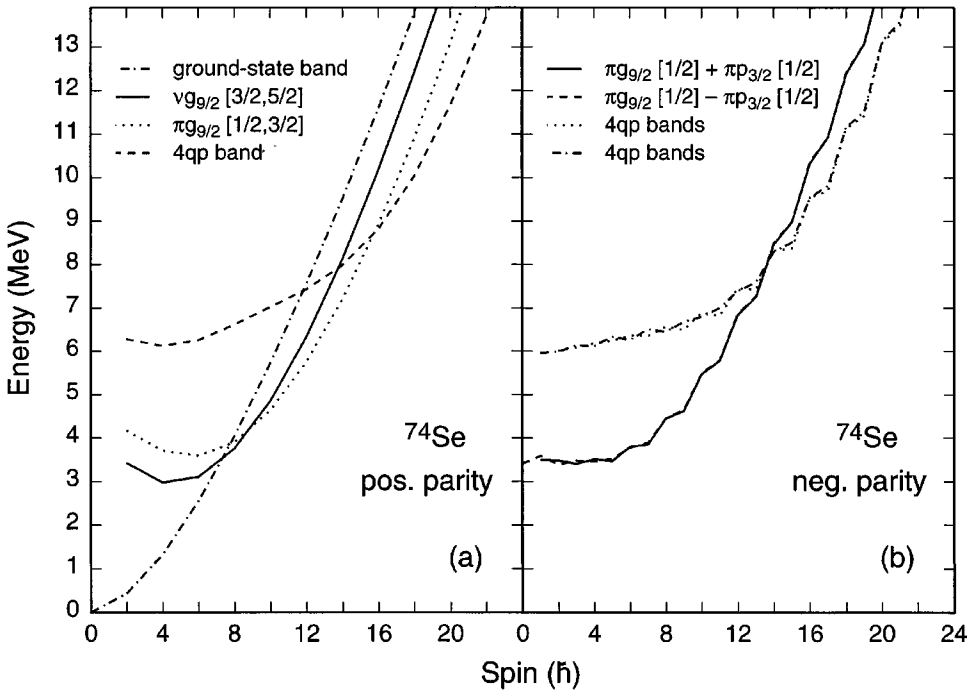

FIG. 9. Calculated excitation energy for positive-parity (a) and negative-parity (b) excitations in ^{74}Se using the projected shell model. Note that the two 2qp negative-parity bands are nearly degenerate in energy, as are the two 4qp bands.

first achieved within the quasiparticle basis with respect to the deformed BCS vacuum $|\phi\rangle$, then rotational symmetry is restored for these states by standard projection technique [29] to form a spherical basis in the laboratory frame, and finally the shell-model Hamiltonian is diagonalized in this basis. The truncation obtained in this way is very efficient. Usually, quite satisfactory results can be obtained by choosing only a few quasiparticle orbitals near the Fermi surface, because the quasiparticle basis already contains most of the pairing and quadrupole correlations [28].

The vacuum $|\phi\rangle$, is determined by the diagonalization of a deformed Nilsson Hamiltonian and a subsequent BCS calculation. Hereby the standard Nilsson scheme [30] is used for the deformed single-particle calculation. The configuration space includes three major shells, $N=2$, 3, and 4, for both neutrons and protons. The Hamiltonian employed in this work is [28]

$$\hat{H}=\hat{H}_0-\frac{1}{2}\chi\sum_{\mu}\hat{Q}^{\dagger}_{\mu}\hat{Q}_{\mu}-G_M\hat{P}^{\dagger}\hat{P}-G_Q\sum_{\mu}\hat{P}^{\dagger}_{\mu}\hat{P}_{\mu}, \quad (1)$$

where $\hat{H}_0$ is the spherical single-particle shell-model Hamiltonian and the other terms are quadrupole-quadrupole, monopole-, and quadrupole-pairing interactions, respectively. The strength of the quadrupole-quadrupole force χ is adjusted in such a way that the employed quadrupole deformation ϵ_2 is obtained as a result of the Hartree-Fock-Bogoliubov self-consistent procedure. Thus all the bands shown here have a fixed deformation which has been chosen to be $\epsilon_2=0.29$. The monopole-pairing force constants G_M used in the calculations are

$$G_M^n=\left[20.25-16.20\frac{N-Z}{A}\right]A^{-1}, \quad G_M^p=20.25A^{-1}. \quad (2)$$

These constants were taken from Ref. [31] with a scaling factor of 0.9. The scaling factor was introduced because our single-particle basis is larger than theirs. (We would like to mention that the monopole-pairing forces chosen here may not be the optimal ones.) Finally, the strength parameter G_Q for the quadrupole pairing was simply taken to be proportional to G_M. For the present calculation a value of 0.16 was chosen which is consistent with the value used in other mass regions [28].

2. Results

In the $A=80$ mass region, both quasineutrons and quasiprotons occupy the same shell-model configuration space. This is a remarkable difference compared with rare-earth nuclei. In the rare-earth region, the neutron alignment is usually favored since the neutron intruder orbital has a higher j quantum number. One usually does not observe a proton alignment prior to the neutron alignment, i.e., a proton aligned band cannot become yrast. In the present case, however, the situation is different. Neutrons and protons can occupy the same orbitals, and it is not obvious, *a priori*, which alignment will be favored. This will depend on the individual case and critically depends on the orbitals at the Fermi surface.

In ^{74}Se, we found that the neutron Fermi level lies between the Nilsson orbitals with $K=\frac{3}{2}$ and $\frac{5}{2}$ of $\nu g_{9/2}$ and also close to $K=\frac{3}{2}$ of $\nu f_{5/2}$, and the proton one between $K=\frac{1}{2}$ and $\frac{3}{2}$ of $\pi g_{9/2}$ and also close to $K=\frac{1}{2}$ of $\pi p_{3/2}$. For the positive-parity states, the lowest-lying neutron 2qp configuration

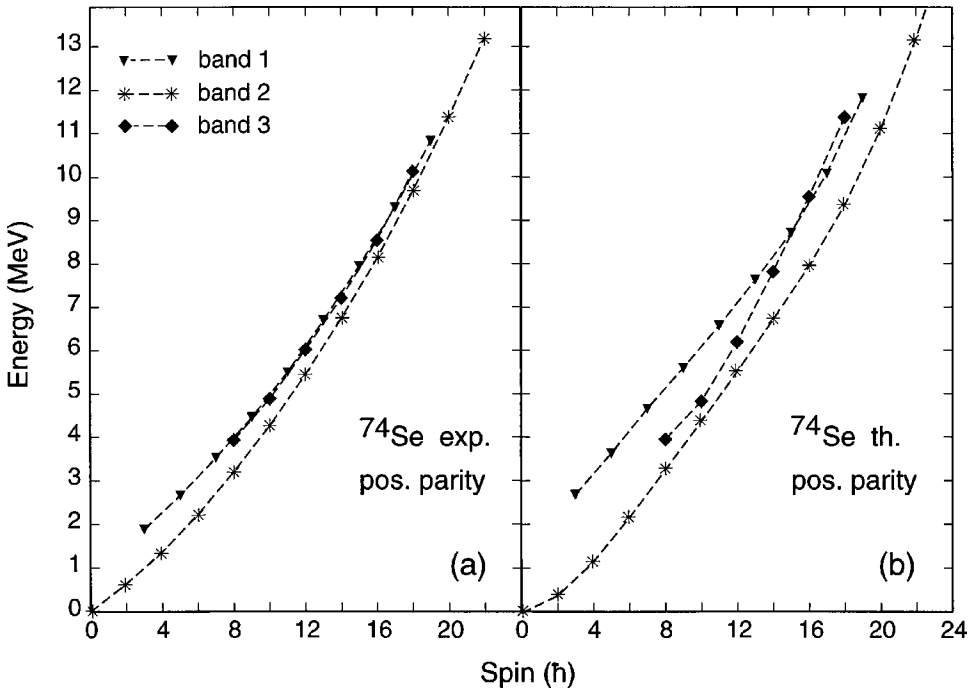

FIG. 10. Comparison of experimental (a) and theoretical (b) excitation energies for positive-parity bands in ^{74}Se.

must be the one based on $[\frac{3}{2}g_{9/2},\frac{5}{2}g_{9/2}]$ neutrons and the lowest-lying proton 2qp configuration on $[\frac{1}{2}g_{9/2},\frac{3}{2}g_{9/2}]$ protons. Their combination gives the lowest 4qp state, a state with both aligned quasineutron and quasiproton pairs. For the negative-parity states, two sets of configurations lie nearly at the same lowest energy: One is the most favored 2qp configuration of a neutron pair $[\frac{5}{2}g_{9/2},\frac{3}{2}f_{5/2}]$. By adding a quasiproton pair $[\frac{1}{2}g_{9/2},\frac{3}{2}g_{9/2}]$ to this neutron 2qp configuration, one can have a favored 4qp state of negative parity. The other one is the most favored 2qp configuration of a proton pair $[\frac{1}{2}g_{9/2},\frac{1}{2}p_{3/2}]$. By adding a quasineutron pair $[\frac{3}{2}g_{9/2},\frac{5}{2}g_{9/2}]$ to this proton 2qp configuration, one can have another favored 4qp state of negative parity.

In Fig. 9 the band diagram for ^{74}Se is shown, which is characteristic for this mass region. Note that this figure is calculated without an interaction between the bands. On the left-hand side of this figure the positive-parity bands with even spins are illustrated. Four bands are plotted so one can see how they behave as a function of spin, although more

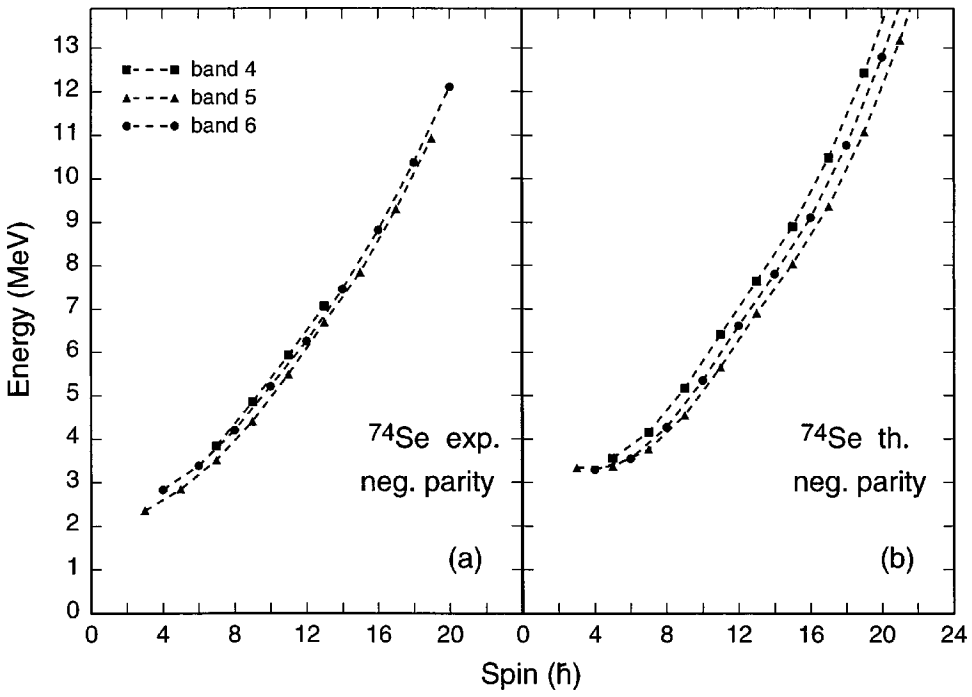

FIG. 11. Comparison of experimental (a) and theoretical (b) excitation energies for negative-arity bands in ^{74}Se.

bands are included in the calculation. The ground-state band increases monotonically, showing a pure rotational behavior. The 2qp bands, both for quasineutrons and quasiprotons, go first downwards, bend at the minimum and then go up. This kind of behavior [32] is analogous to the decoupling effect [33] in the particle-rotor model. Because of this, 2qp bands can cross with the ground-state band and become yrast.

Figure 9(a) clearly shows three band crossings along the yrast line: two of them around spin 8 and one close to spin 16. Here, one can see that the band with a $g_{9/2}$ quasineutron pair, which lies about 3 MeV above the ground-state band at the beginning, crosses with the ground-state band before spin 8 and becomes yrast after the crossing. The $g_{9/2}$ quasiproton pair, which is located about 1 MeV higher than the $g_{9/2}$ quasineutron one at the beginning, comes down and crosses first with the ground-state band and then with the neutron 2qp band just after spin 8, becoming yrast for the spin region 10 to 14. The 4qp state becomes yrast at spin around 16 where it crosses with the proton 2qp band.

Thus, the first peak in $J^{(2)}$ of the yrast band (see band 2 in Fig. 5) should be due to a nearly simultaneous crossing of neutron and proton 2qp states with the ground-state band around spin 8. The second one in this band is due to the 4qp-band crossing with the proton 2qp band around spin 16. The measured third peak cannot be reproduced within the present model space. However, it is expected that another band crossing with a 6qp configuration will occur around spin 22. The reason for not reproducing that experimental peak is that 6qp configurations have not been included in the present calculations.

The band diagram for negative-parity bands in ^{74}Se is displayed in Fig. 9(b). Of the 2qp neutron and proton configurations discussed above, we found that the two-quasiproton configuration at lower spins and the 4qp configuration (with a quasineutron pair added to this two-quasiproton state) at higher spins dominate the observed negative-parity bands 4, 5, and 6. The reason is that only these configurations show the staggering character because these states have smaller K quantum numbers. On the other hand, no staggering is found in the 2qp-neutron state and the corresponding 4qp state has a larger K number. Although they are all included in the configuration mixing, the relevant 2qp-proton and the corresponding 4qp states are plotted in Fig. 9(b) only for an easier reading of this figure.

The quasiproton pair $[\frac{1}{2}g_{9/2}, \frac{1}{2}p_{3/2}]$ can be coupled to states having a total $K=0$ and 1, and the two corresponding bands can have a similar bandhead energy. As one can see from Fig. 9(b), these two bands behave similarly as a function of spin, and in fact, they are nearly degenerate. Around spin 13, 4qp bands come into play, which have a structure of the present proton 2qp configuration plus a quasineutron pair of $[\frac{3}{2}g_{9/2}, \frac{5}{2}g_{9/2}]$. They cross the 2qp bands and become lower in energy. This explains, in general, the observed anomaly in the dynamic moments of inertia, $J^{(2)}$, of the negative-parity bands shown in Fig. 7. At very low spins, the 2qp bands show a flat behavior as a function of spin, and a strong interaction with other 2qp states not shown in the plot.

The final results to be compared with data are obtained by diagonalization of the Hamiltonian given in Eq. (1). Bands discussed above are thus more or less mixed by this procedure, i.e., in a strict sense, they no longer have the pure configurations shown above. All the bands discussed in the following are obtained by one diagonalization which contains about 100 configurations in the mixing. The theoretical results for the positive-parity bands are compared with experimental data in Fig. 10. The numbers used to denote the bands are identical to those in Fig. 1. The yrast band (band 2) is very well described by the theory. The predicted first excited band (even-spin sequence) agrees well with the measured one, band 3, up to the first band crossing, but not for states at higher spins. The lowest odd-spin band is calculated theoretically too high in energy, when compared with the measured one, band 1. Two possible points could lead to these deviations. First, bands 1 and 3 could have different deformations compared to band 2, as was discussed for low-lying states a long time ago [2] in terms of shape coexistence. Secondly, TRS calculations suggest a non-negligible γ-deformation for both low- and high-spin states in this nucleus. In our calculation, the deformed states are constructed at a fixed deformation ($\epsilon_2 = 0.29$) with axial symmetry. Although our model is a shell model in nature, it can take care of shape fluctuations around a certain deformation through configuration mixing. It seems that this is not enough to account for the various shape changes in the present case. Inclusion of the γ degree of freedom in the deformed states could improve the agreement but this requires three dimensional projection of angular momentum. Clearly, the present data pose a challenge to the theoretical model.

Finally, theoretical results for the negative-parity bands are compared with experimental data in Fig. 11. The two degenerate states from the different coupling schemes shown in Fig. 9 are now pushed apart by interactions between them. Clear signature splitting can be seen: the bands separate into two $\Delta I = 2$ sequences. The theoretical results are a little too high in energy for the first states in the calculated bands when compared with experimental bandhead energies of bands 5 and 6. Nevertheless, they show a correct description for higher-spin states and suggest that these bands have a structure as shown in Fig. 9(b). The calculated bands also show a signature splitting similar to that deduced from the experiment, suggesting that bands 5 and 6 are signature partners.

V. SUMMARY

New results for low- and high-spin states in ^{74}Se studied via the ^{65}Cu(^{12}C, $p2n$)^{74}Se reaction were presented, leading to modified spin and parity assignments for a few low-lying states and to different moments of inertia for the yrast high-spin states when compared with the previous level scheme. In particular, a recent nuclear orientation measurement and the present DCO ratios suggest a return to the earlier spin and parity assignments of 3^+ for the 1884.0 keV state, leading to a firm odd-spin level sequence of positive parity in band 1.

The known irregularity in the kinematic moments of inertia at the 10^+ yrast state and the behavior in the spin range 10 to 16 can mainly be ascribed to the influence of a $g_{9/2}$ quasiproton band if an axial-deformed prolate shape is assumed. Projected shell-model calculations support this sce-

nario. Thus, the new positive-parity band 3 which is built on the (8_2^+) state at 3928.6 keV can be related to a $g_{9/2}$ quasineutron excitation at the beginning. At about spin 16 the yrast band and band 3 are crossed by a 4qp band containing both $g_{9/2}$ quasiproton and $g_{9/2}$ quasineutron excitations.

The lowest states of the even-spin and odd-spin bands of negative parity, bands 5 and 6, known to show octupole correlations, are interpreted in the framework of the projected shell model as $g_{9/2}$ quasiproton excitations before crossing. At higher rotational frequency the bands are influenced by a $g_{9/2}$ quasineutron pair alignment leading to 4qp excitations.

ACKNOWLEDGMENTS

The participation of J. W. Holcomb, T. D. Johnson, and P. C. Womble in the early stage of this project is acknowledged. We thank J. X. Saladin from the University of Pittsburgh for his many contributions to the combined Pitt-FSU Ge detector array. We are grateful to P. Cottle and W. Nazarewicz for fruitful discussions, and to R. Wyss for providing the TRS computer codes. This work was supported in part by the U. S. National Science Foundation under Contract Nos. PHY-9210082 with Florida State University and PHY94-02761 with University of Notre Dame.

[1] R. M. Lieder and J. E. Draper, Phys. Rev. C **2**, 531 (1970).
[2] J. H. Hamilton, A. V. Ramayya, W. T. Pinkston, R. M. Ronningen, G. Garcia-Bermudez, H. K. Carter, R. L. Robinson, H. J. Kim, and R. O. Sayer, Phys. Rev. Lett. **32**, 239 (1974).
[3] M. L. Halbert, P. O. Tjøm, I. Espe, G. B. Hagemann, B. Herskind, M. Neiman, and H. Oeschler, Nucl. Phys. **A259**, 496 (1976).
[4] R. M. Ronningen, A. V. Ramayya, J. H. Hamilton, W. Lourens, J. Lange, H. K. Carter, and R. O. Sayer, Nucl. Phys. **A261**, 439 (1976).
[5] R. B. Piercey, A. V. Ramayya, R. M. Ronningen, J. H. Hamilton, R. L. Robinson, and H. J. Kim, Phys. Rev. Lett. **37**, 496 (1976).
[6] K. P. Lieb and J. J. Kolata, Phys. Rev. C **15**, 939 (1977).
[7] R. B. Piercey, A. V. Ramayya, R. M. Ronningen, J. H. Hamilton, V. Maruhn-Rezwani, R. L. Robinson, and H. J. Kim, Phys. Rev. C **19**, 1344 (1979).
[8] C. J. Gross, P. D. Cottle, D. M. Headly, U. J. Hüttmeier, E. F. Moore, and S. L. Tabor, Phys. Rev. C **36**, 2127 (1987).
[9] J. Adam, M. Honusek, A. Špalek, D. N. Doynikov, A. D. Efimov, M. F. Kudojarov, I. Kh. Lemberg, A. A. Pasternak, O. K. Vorov, and U. Y. Zhovliev, Z. Phys. A **332**, 143 (1989).
[10] P. D. Cottle, J. W. Holcomb, T. D. Johnson, K. A. Stuckey, S. L. Tabor, P. C. Womble, S. G. Buccino, and F. E. Durham, Phys. Rev. C **42**, 1254 (1990).
[11] T. Mylaeus, J. Busch, J. Eberth, M. Liebchen, R. Sefzig, S. Skoda, W. Teichert, M. Wiosna, P. von Brentano, K. Schiffer, K. O. Zell, A. V. Ramayya, K. H. Maier, H. Grawe, A. Kluge, and W. Nazarewicz, J. Phys. G **15**, L135 (1989).
[12] J. C. Wells, Jr., R. L. Robinson, H. J. Kim, R. O. Sayer, R. B. Piercey, A. V. Ramayya, J. H. Hamilton, and C. F. Maguire, Phys. Rev. C **22**, 1126 (1980).
[13] T. Matsuzaki and H. Taketani, Nucl. Phys. **A390**, 413 (1982).
[14] R. Schwengner, G. Winter, J. Döring, L. Funke, P. Kemnitz, E. Will, A. E. Sobov, A. D. Efimov, M. F. Kudojarov, I. Kh. Lemberg, A. S. Mishin, A. A. Pasternak, L. A. Rassadin, and I. N. Chugunov, Z. Phys. A **326**, 287 (1987).
[15] S. L. Tabor, M. A. Riley, J. Döring, P. D. Cottle, R. Books, T. Glasmacher, J. W. Holcomb, J. Hutchins, G. D. Johns, T. D. Johnson, T. Petters, O. Tekyi-Mensah, P. C. Womble, L. Wright, and J. X. Saladin, Nucl. Instrum. Methods Phys. Res. B **79**, 821 (1993).
[16] K. S. Krane, R. M. Steffen, and R. M. Wheeler, Nucl. Data Tables **11**, 351 (1973).
[17] A. Krämer-Flecken, T. Morek, R. M. Lieder, W. Gast, G. Hebbinghaus, H. M. Jäger, and W. Urban, Nucl. Instrum. Methods Phys. Res. A **275**, 333 (1989).
[18] N. Yoshikawa, Y. Shida, O. Hashimoto, M. Sakai, and T. Numao, Nucl. Phys. **A327**, 477 (1979).
[19] C. G. Barham, S. S. Alghamdi, A. Bhagwat, M. Booth, I. S. Grant, M. Lindroos, J. Rikovska, B. D. D. Singleton, N. J. Stone, and P. M. Walker, Hyperfine Interact. **75**, 433 (1992).
[20] J. Döring, G. D. Johns, R. A. Kaye, M. A. Riley, S. L. Tabor, P. C. Womble, and J. X. Saladin, Phys. Rev. C **52**, R2284 (1995).
[21] A. R. Farhan, Nucl. Data Sheets **74**, 529 (1995).
[22] M. Borsaru, D. W. Gebbie, J. Nurzynski, C. L. Hollas, L. O. Barbopoulos, and A. R. Quinton, Nucl. Phys. **A284**, 379 (1977).
[23] J. Barrette, M. Barrette, G. Lamoureux, S. Monaro, and S. Markiza, Nucl. Phys. **A235**, 154 (1974).
[24] R. Bengtsson and S. Frauendorf, Nucl. Phys. **A327**, 139 (1979).
[25] J. Heese, N. Martin, C. J. Gross, W. Fieber, K. P. Lieb, A. Kuhnert, K. H. Maier, and X. Sun, Phys. Rev. C **41**, 1553 (1990).
[26] T. D. Johnson, T. Glasmacher, J. W. Holcomb, P. C. Womble, S. L. Tabor, and W. Nazarewicz, Phys. Rev. C **46**, 516 (1992).
[27] W. Nazarewicz, J. Dudek, R. Bengtsson, T. Bengtsson, and I. Ragnarsson, Nucl. Phys. **A435**, 397 (1985).
[28] K. Hara and Y. Sun, Int. J. Mod. Phys. E **4**, 637 (1995).
[29] P. Ring and P. Schuck, *The Nuclear Many-Body Problem* (Springer-Verlag, New York, 1980).
[30] T. Bengtsson and I. Ragnarsson, Nucl. Phys. **A436**, 14 (1985).
[31] W. Dietrich, A. Bäcklin, C. O. Lannergård, and I. Ragnarsson, Nucl. Phys. **A253**, 429 (1975).
[32] K. Hara and Y. Sun, Nucl. Phys. **A529**, 445 (1991).
[33] A. Bohr and B. R. Mottelson, *Nuclear Structure*, Vol. I (Benjamin, New York, 1969).